EXPERIMENTAL STDUY ON SLENDER RECTANGULAR RC WALLS (PART II: ANALYSIS)

Slender Wall　Flexural Failure　Ultimate drift
High Axial Load　Fiber Model

○Chanipa NETRATTANA*1　Tatsuya TAKAHASHI*1
Taku OBARA*1　Susumu KONO*1
David MUKAI*2

1 Introduction

Behavior of four specimens until their ultimate drift points were dominated by flexure mode. In part II, load-drift relations and the ultimate drift are simulated by a fiber based model.

2 Model description

The experimental results were simulated by a fiber based model. This model includes flexural deformation as shown in section 2.1 and shear deformation as shown in section 2.2. Ultimate point was assessed by ultimate confined concrete limit strain in section 3.3.

2.1 Material properties

Concrete and steel material model is presented in Fig. 1. The modified Kent and Park model provided a monotonic envelope curve for concrete in compression [1]. Confined concrete strength was estimated by Chang et al. [2]. Unloading and reloading paths followed Karsan and Jirsa [3] model. A nonlinear hysteretic steel model proposed by Menegotto-Pinto [4] was used.

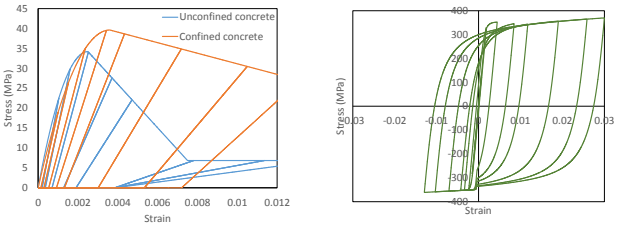

(a) Concrete model　(b) Steel model

Fig.1 Stress-strain relation for concrete and steel

2.2 Flexural drift

Flexural deformation was assumed to be a combination of elastic deformation and plastic deformation as shown in Fig. 2 (a) and Eq.(1). To calculate plastic deformation, plastic curvature was assumed to distribute constantly over a plastic hinge length, l_p. Plastic hinge length was assumed to be 0.5 of wall length.

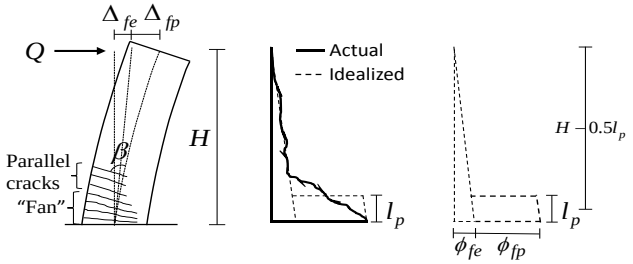

(a) Flexural deformation　(b) Idealized curvature distribution　(c) Elastic and plastic curvature distribution

Fig.2 Flexural drift component

$$R_f = R_{fe} + R_{fp} = \frac{1}{H_c}\left(\Delta_{fe} + \Delta_{fp}\right) \quad (1)$$

where Δ_{fe}: flexural elastic deformation, Δ_{fp}: flexural plastic deformation, H_c: Height to contraflexure point.

2.3 Shear drift

Shear deformation for wall controlled by flexure was estimated as Eq.(2) which proposed by Beyer et al. [5]. The cracking angle, β, is the cracking angle in plastic zone above fan cracks region where cracks are approximately parallel as shown in Fig. 2 (a).

$$\frac{R_s}{R_f} = 1.5\frac{\varepsilon_{mean}}{\varphi \tan\beta}\frac{1}{H_c} \quad (2)$$

where ε_{mean}: axial strain at center of wall section, φ: curvature, β: crack angle assumed to be 45 degrees, H_c: Height to contraflexure point.

2.4 Ultimate drift

Analytical ultimate point was determined when extreme concrete fiber reached ultimate confined concrete limit strain, ε_{cu}. The ultimate limit strain for confined concrete can be estimated with Eq.(3) [6]. To estimate ultimate drift capacity, a confined rebar strain at ultimate point, ε_m was assumed to be 2%.

$$\varepsilon_{cu} = 0.004 + 1.4\frac{\rho_s f_{yh}\varepsilon_m}{f'_{cc}} \quad (3)$$

where ρ_s : confined reinforcement volume to confined concrete volume ratio, f_{yh}:confined reinforcement yield strength, ε_m: confined reinforcement strain at ultimate point, f'_{cc}: confined concrete strength.

3 Comparison of experimental and analytical load-drift relation and ultimate drift

Figure 3 (a-d) in part I shows comparison of experimental and analytical load-drift relation and ultimate drift. The model well simulated the load-drift relation of four specimens. However, residual drifts were underestimated for RW20, RW20T and RW20C. Zhang [7] used a concrete model considering crack closure effect, and similar model should be considered for better estimation of residual drift of RC walls under cyclic loading.

Load degradation after maximum load was well simulated in RW20, RW20C and RW40 until the ultimate drift. For RW20T, load degradation after maximum load in experiment was larger than that of the model. The reason might be buckling of longitudinal reinforcement, thinner cover concrete than other specimens and thinner wall thickness which induced damage to concrete around it. When longitudinal reinforcement buckles, compressive stress is redistributed to concrete around the

reinforcement, and these concrete tends to be damaged. Based on the experimental results in part I, stiffness of load degradation of RW20T was significant larger than RW20.

The model captured small ultimate drift of RW40 due to high axial load. Analytical ultimate drift of RW20T and RW20C were larger than RW20 because of larger amount of confining reinforcement ratio. Figure 4 shows that the model estimated the ultimate drift capacities of four specimens within 20% error, although RW20C had 24 % error. From Fig. 7 part I, concrete at boundary region in RW20C was much confined than that of RW20, especially between R=-1.5 % to R=-2.0 %. Degradation path of modified Kent and Park model for concrete may not reflect stress degradation of confined concrete in RW20C.

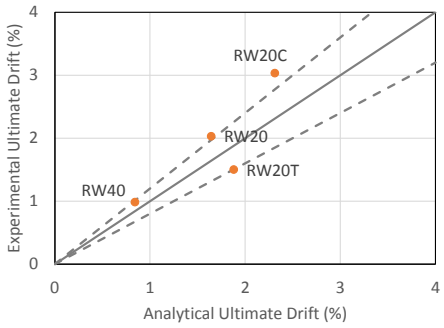

Fig.3 Comparison of experimental and analytical ultimate drift capacity

4 Conclusions

The model with assumptions 1) plastic hinge length is 0.5 of wall length and 2) confined rebar strain of 2% was able to simulate lateral load-drift relation and ultimate point for four specimens. The ultimate drift capacity of RC wall with additional hoop and tie reinforcement was underestimated. For RC wall with 100 mm thickness, the model overestimated load for post-peak portion.

5 Acknowledgments

This study was supported financially by "SOFTech" and JSPS Grant-in-Aid program (PI: Susumu Kono). We are thankful to CRP of MSL, WRHI at Tokyo Institute of Technology and MEXT scholarship.

6 References

1) Scott, B.D., Park, R., and Priestley M.J.N. (1982). Stress-strian behavior of concrete confined by overlapping hoops at low and high strain rates. *ACI Structural Journal*, 79(1), 13-27.
2) Karan, I.D. and Jirsa, J.O. (1969). Behavior of concrete under compressive loadings. *ASCE Journal of Structural Engineering*, 95(12), 2543-2563.
3) Chang, Y.Y., Deng, H.Z., Lau, D.T., Ostovari, S., Tsai, K.C. and Khoo, H.A. (2004). A simplified method for nonlinear cyclic analysis of reinforced concrete structures: direct and energy based formulations. *Proceedings of the 13th World Conference on Earthquake Engineering*, Vancouver, Canada
4) Menegotto, M. and Pinto, E. (1973). Method of analysis for cyclically loaded reinforced concrete plane frames including changes in geometry and non-elastic behavior of elements under combined normal force and bending. *Proceedings of IABSE Symposium on Resistance and Ultimate Deformability of Structures Acted on by Well-Defined Repeated Loads*, Lisbon, Portugal.
5) Beyer, K., Dazio, A. and Priestley, M.J.N. (2011). Shear deformations of slender reinforced concrete walls under seismic loading. *ACI Structural Journal*, 108(2), 167-177.
6) Paulay T. and Priestley M.J.N. (1992). Seismic design of reinforced concrete and masonry building. New York, John Wiley & Sons.
7) Zhang, L. (2020). Numerical analysis tool for modelling reinforced concrete shear wall buildings subject to earthquake loading. University of Canterbury, Christchurch, New Zealand

*1 Tokyo Institute of Technology
*2 University of Wyoming